

Supplementary Materials

Introduction

Text S1 describes the specifications of an algorithm used for estimating melt pond fraction (MPF) using the Advanced Microwave Scanning Radiometer-Earth observing system (AMSR-E MPF) [21]. Text S2 describes evaluation of the limitations of the AMSR-E MPF estimates in [21] and the need for additional evaluation on a day-by-day basis. Text S3 helps the main sources of error in the ice charts described in [25]. Text S4 describes specifications (such as performance and limitation) of the MPF from the Medium Resolution Imaging Spectrometer (MERIS) data [26,27].

Table 1 provides a numerical summary of DO and DD in Figures 8 and 9 of the manuscript.

Figure S1 shows spatial distributions of melt onset (MO) in the Canadian Arctic Archipelago (CAA) from 2006 to 2011.

Text S1

The AMSR-E MPFs in this study are retrieved from the L3 25-km T_B product (Subsection 2.2) using the AMSR-E MPF algorithm [21]. Data computed by the algorithm can be seen in [21]. This text gives a brief overview of the AMSR-E MPF algorithm. The AMSR-E MPF algorithm is proposed based on the ship-based MPF retrieved using an image analysis method based on forward-looking camera images observed from July to August. First, researchers examined the effect of MPF over areas with sea ice concentrations exceeding 95% on T_B , as it is difficult to examine areas with lower ice concentrations because the frequencies used are less affected by salinity and due to the difficulty of distinguish between saline seawater and freshwater in the ponds in cold water regions [32,33]. The authors found T_B with H and V polarizations of 6.9 GHz (T_{B06H}) and 89.0 GHz (T_{B89V}), respectively, to be very sensitive to MPF over areas with sea ice concentrations exceeding 95%. The gradient ratio between T_{B06H} and T_{B89V} ($GR_{06H-89V}$) depends on the MPF, which is called the melt pond index ($MP_{06H-89V}$) by [21]. They found the AMSR-E MPF algorithm to be useful (1) over areas with high sea ice concentrations, (2) from July to August towards third melt season, and (3) in areas with low atmospheric influence.

[21] defined the gradient ratio $GR_{06H-89V}$, as expressed in Equation (1) below.

$$GR_{06H-89V} = \frac{T_{B06H} - T_{B89V}}{T_{B06H} + T_{B89V}} \quad (1)$$

$GR_{06H-89V}$ showed better sensitivity than other channel combinations when compared with ship-based MPF. Equation (2) below calculates the MPF on the Arctic sea ice surface, which is retrieved by the regression of the ship-based MPF observations and $GR_{06H-89V}$.

$$\text{MPF [\%]} = 15.2 - 158.9GR_{06H-89V} \quad (2)$$

This equation is useful in areas with MPF from 0 to 65%, and first-year ice (FYI) (particularly medium and thick) and multi-year ice (MYI).

Text S2

The previous evaluation of the AMSR-E MPF [21] was limited to an inter-comparison with an 8-day composite MPF from the Moderate Resolution Image Spectrometer (MODIS MPF) [15], which is a bias-corrected version 2 product. [15] reported that the bias of the AMSR-E MPF was less than 5% in most regions, and periods as compared to the 8-day composite MODIS MPF [15]. This showed that the AMSR-E MPF algorithm obtains a product of comparable quality to the 8-day composite MODIS MPF [21]. Using the MODIS MPF, it is difficult to evaluate the AMSR-E algorithm on day-by-day basis since the MPF peaks during 4–6 days in the first melt season and is close to its minimum during the first 5–7 days in the second melt season [8,9,11]. The DO timing differs in sea ice conditions and regions. Since our focus in this study provides the DO timing and DD based on time series of the daily MPF, additional evaluation on a day-by-day basis is needed.

Text S3

The main shortcoming of the ice charts is the varying error with space and time. The accuracy of an ice chart is very dependent on the adapted data source. As the RADARSAT-1 SAR began observing in 1996, more than 80% of the sources of the ice charts are from RADARSAT-1 and 20% from nowcasting [25]. The errors in ice concentration are 5% for RADARSAT-1 and 10–30% for nowcasting, which are less than 40% for the Special Sensor Microwave Imager (SSM/I). In addition, classification between FYI and MYI can be performed by using RADARSAT-1 [25]. The ice charts analyst estimates ice type from the tone, texture and shapes in the SAR imagery. For instance, use of the imagery can easily classify ice types as FYI or MYI. This is because the high backscatter results from volume scattering by large air inclusions within the ice, so that MYI is bright in the imagery in most cases. Moreover, C-band (around 5 GHz) SAR mounted on the RADARSAT satellite provides good classification between sea ice (types) and open water during the melt season [34,35]. This ice chart is little used information of the RADARSAT SAR observation, most intervals of which are 2–4 days for our study. This study focuses on the CAA, which is a region with fast ice. Therefore, we can identify the totally ice-covered area until the breakup of fast ice. The U.S. National Ice Center (NIC) weekly ice chart over the pan-Arctic on the NSIDC web site can be also used, but this NIC chart includes observations from passive microwave.

Text S4

The broadband albedo is retrieved as an average of the six spectral albedo values at 400–900 nm at 100 nm intervals. The MPD algorithm is very different from a-priori fixed values of the spectral reflection coefficients such as snow, bare ice, melt ponds, and open water [15,36] and adapts the spectral signature of melt ponds in the measured top of the atmosphere signal. Typically, the light blue (young) and dark (mature) ponds correspond to ponds over MYI or thicker ice and over FYI or thinner ice, respectively. The melt pond detector (MPD) algorithm can obtain a more accurate MERIS MPF on ice with a blue pond than with a dark pond. And the MERIS MPF is underestimated more than twice in the case of bright (snow-covered) ice and dark ponds [16]. This is, however, is a rare case where events occur in a short time as the appearance of open mature ponds and snowfall. Moreover, the MERIS MPF is overestimated because the reflectance of a wet or water-saturated surface or thin ice is very close to that of a melt pond [16]. [26] also evaluated the performance of the MPD algorithm using in situ measurement, ship-borne, and aerial-borne data. The retrieved MERIS MPF is overestimated before melt onset and underestimated after melt onset. The MPD algorithm is particularly more accurate on land-fast ice and MYI. Error over an area with FYI in pack ice ranges from 18% to 38% [26] but our study focuses on land-fast ice. The MPD algorithm is needed to determine valid pixels by cloud screening because the Arctic region during summer is subject to up to 80% cloud cover. The greatest influence of unscreened clouds (up to 15% MPF bias) on the surface before melt onset and later is being close to dark due to snow/ice melt [27]. This means that the bias in MERIS MPF occurred by unscreened clouds decreases.

Table S1. Summary of the melt onset, drainage onset, and drainage duration in the entire CAA and seven sub-regions averaged from 2006 to 2011. SD means standard deviation.

Region	Region area [km ² × 10 ⁶]	MO		DO		DD	
		Average [DOY]	SD [days]	Average [DOY]	SD [days]	Average [DOY]	SD [days]
All	19.3	153	9	177	9	13	9
Queen Elizabeth Islands	5.5	156	7	182	11	17	7
W. Parry Channel	3.4	154	9	177	8	13	9
E. Parry Channel	1.1	157	6	177	6	10	9
M Clintock	1.3	153	9	178	4	16	7
Franklin	1.2	154	10	175	4	14	8
Baffin Inlet	2.6	151	9	174	7	9	11
W. Arctic Waterway	4.2	149	10	171	6	11	10

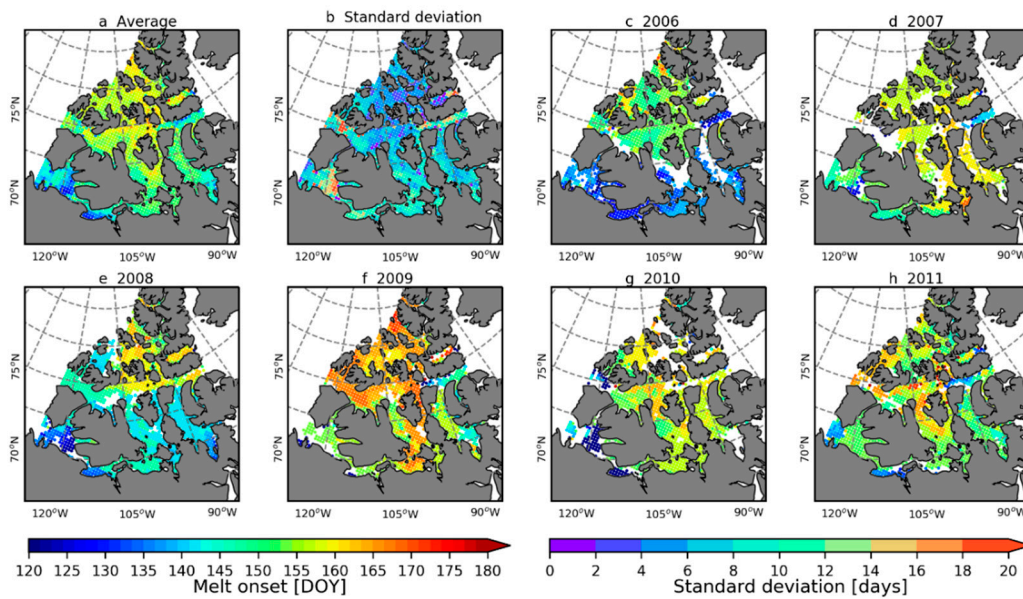


Figure S1. Spatial distributions of the melt onset in the Canadian Arctic Archipelago from 2006 to 2011. The melt onset is in day of year (DOY).

References

31. Ulaby, F.; Long, D.G. *Microwave Radar and Radiometric Remote Sensing*; University of Michigan Press: Ann Arbor, MI, USA, 2014.
32. Ulaby, F.T.; Moore, R.K.; Fung, A.K. *Microwave Remote Sensing: Active and Passive, Vol. III: Microwave Remote Sensing Fundamentals and Radiometry*; Artech House, Norwood, MA, USA, 1986; pp. 1417–1434.
33. Meissner, T.; Wentz, F.J. The emissivity of the ocean surface between 6–90 GHz over a large range of wind speeds and Earth incidence angles. *IEEE Trans. Geosci. Remote Sens.* 2012, 50, 3004–3026.
34. Carsey, F.D. *Microwave Remote Sensing of Sea Ice*; American Geophysical Union: Washington, DC, USA, 1992.
35. Geldsetzer, T.; Arnett, M.; Zagon, T.; Charbonneau, F.; Yackel, J.J.; Scharien, R.K. All-season compact-polarimetry C-band SAR observations of sea ice. *Can. J. Remote Sens.* 2015, 41, 485–504.
36. Tschudi, M.A.; Maslanik, J.A.; Perovich, D.K. Derivation of melt pond coverage on arctic sea ice using MODIS observation. *Remote Sens. Environ.* 2008, 112, 2605–2614.